ELSEVIER

Journal of Quantitative Spectroscopy & Radiative Transfer 85 (2004) 35–55

Journal of Quantitative Spectroscopy & Radiative Transfer

www.elsevier.com/locate/jqsrt

The physical parameterization of the top-of-atmosphere reflection function for a cloudy atmosphere—underlying surface system: the oxygen A-band case study

Alexander A. Kokhanovsky[a,b,*], Vladimir V. Rozanov[a]

[a] *Institute of Environmental Physics, Bremen University, P.O. Box 330440, Bremen, Germany*
[b] *Institute of Physics, 70 Skarina Avenue, Minsk 220072, Belarus*

Received 17 December 2002; accepted 17 April 2003

Abstract

The paper is devoted to the physical parameterization of the top-of-atmosphere reflection function. The accuracy of the parameterization is checked against exact radiative transfer calculations in a cloudy atmosphere for various cloud-top-heights, cloud optical and geometrical thicknesses, solar illumination and surface reflection conditions. It was found that the error of approximation is smaller than 5% for most cases studied at the wavelength interval 758–768 nm, which corresponds to the oxygen A-band. This band is routinely used in cloud-top-height retrievals. The model proposed can be used for cloud-top-height and cloud geometrical thickness retrievals. This allows to avoid a standard look-up-table retrieval scheme, involving complex numerical procedures.

Keywords: Radiative transfer; Top-of-atmosphere reflection function; Oxygen A-band

1. Introduction

The radiative transfer in the Earth-atmosphere system is usually studied numerically, solving the well-known integro-differential equation [1]. This is mostly due to the necessity to account for multiple light scattering by aerosol particles and molecules.

The appearance of clouds generally complicates the situation due to the necessity to consider the random structure of cloudiness [2]. On the other hand, the assumption of an optically thick homogeneous plane-parallel cloud layer, which is of importance in most of practical situations [3], leads to the simplification of the problem. This is mostly due to the fact that highly variable reflectance of

* Corresponding author. Tel.: +49-421-218-4475; fax: +49-421-218-4555.
E-mail address: alexk@iup.physik.uni-bremen.de (A.A. Kokhanovsky).

0022-4073/$ - see front matter
doi:10.1016/S0022-4073(03)00193-6

light from the surface and boundary-layer aerosol beneath the cloud plays only a minor role in the total solar light reflectance from cloudy scenes. Thus, they can be accounted for using rather coarse simplifying assumptions and models.

The task of this paper is to propose a simple semi-analytical model for the calculation of the top-of-atmosphere (TOA) reflectance of a underlying surface-atmosphere system, accounting both for aerosol and cloud scattering. The atmospheric gas absorption is also taken into account. Main attention is given to the calculations for the spectral interval, determined by the oxygen A-band (758–768 nm). This band is important for the cloud-top-height determination from spaceborne instruments. Indeed, the reflected light intensity is extremely small in the center of this band for cloudless conditions. This is due to the fact that photons can penetrate down to the underlying surface and be absorbed by oxygen molecules on their way to the surface and back to a receiver. For cloudy atmospheres the situation is different, however. Imagine, that cloud is present at the height 10 km above the ground level. Then most of photons are reflected by the cloud and do not penetrate in the layer underneath the cloud to be absorbed there. This will lead to an increase of reflected light intensity in the center of oxygen A-band as compared to the case of cloudless atmosphere. Clearly, the depth of this line $\mathfrak{J}$ depends on the cloud-top-height. The value of $\mathfrak{J}$ is larger for clouds having smaller cloud-top-heights.

Note that other absorption bands can be employed for the same purpose (e.g., oxygen B-band, O_4 absorption bands, etc.). Our model can be also used to treat all these different cases (both in and out of gaseous absorption bands).

Moreover, the simplified solutions obtained are of importance to clarify the physical processes, which contribute to the TOA reflectance. They can be used also for the development of analytical and semi-analytical cloud retrieval schemes.

2. Theory

The schematic representation of the geometry considered is given in Fig. 1. Unpolarized solar light illuminates the aerosol–gaseous atmosphere in the direction $\vec{\Omega}_0(\vartheta_0, \varphi_0)$ and a receiver detects the reflected light intensity I in the direction, specified by the angle $\vec{\Omega}(\vartheta, \varphi)$. Here ϑ_0 and ϑ are zenith incident and observation angles respectively, φ_0 and φ (not shown in Fig. 1) are correspondent azimuth angles. We will assume that $\varphi_0 = 0$. Then the azimuth difference between incident and reflected beams directions is given by the angle φ.

A cloud layer with top height H and geometrical thickness ΔH (see Fig. 1) is introduced in the aerosol–gaseous atmosphere. Both ΔH and H can be in principle arbitrary. However, we assume that $\Delta H \geqslant 5l$, where l is the photon free path length in a cloud. For a typical value $l = 20$ m, it follows: $\Delta H \geqslant 100$ m.

It means that only cases of optically thick clouds with the optical thickness $\tau_c \equiv \Delta H/l \geqslant 5$ are considered. Note, that thinner clouds are highly inhomogeneous both in vertical and horizontal directions. Therefore, the model of a plane-parallel homogeneous cloud layer is characterized by a large uncertainty for thinner clouds. We avoid these difficulties, assuming from the very beginning that $\tau_c \geqslant 5$. The surface is assumed to be Lambertian with albedo A.

The TOA reflectance $R_{\Delta\lambda}(\vartheta_0, \vartheta, \varphi)$, measured by a radiometer or spectrometer with a spectral resolution $\Delta\lambda$, is related to the reflected monochromatic light intensity $I(\lambda, \vartheta_0, \vartheta, \varphi)$ by the following

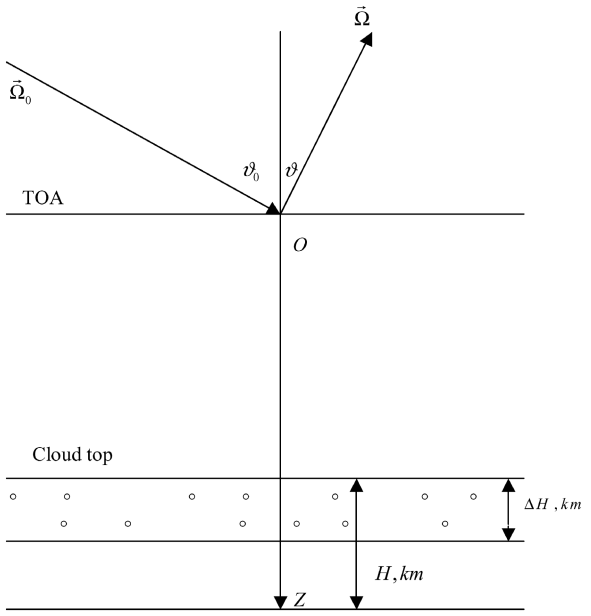

Fig. 1. The geometry of the problem.

relationship [1]:

$$R_{\Delta\lambda}(\vartheta,\vartheta_0,\varphi)=\frac{I_{\Delta\lambda}(\vartheta,\vartheta_0,\varphi)}{F_{\Delta\lambda}\cos\vartheta_0}, \tag{1}$$

where

$$I_{\Delta\lambda}(\vartheta_0,\vartheta,\varphi)=\int_{\lambda-\Delta\lambda/2}^{\lambda+\Delta\lambda/2} f(\lambda,\lambda')I(\lambda',\vartheta_0,\vartheta,\varphi)\,\mathrm{d}\lambda', \quad \int_{\lambda-\Delta\lambda/2}^{\lambda+\Delta\lambda/2} f(\lambda,\lambda')\,\mathrm{d}\lambda'=1,$$

where $f(\lambda,\lambda')$ is the radiometer spectral response function and $\pi F_{\Delta\lambda}\cos\vartheta_0$ is the incident solar flux density on the TOA in the spectral range $\Delta\lambda$. Value (1) is routinely measured by various radiometers and spectrometers, placed on satellite platforms [4].

The shape and half-width of the function $f(\lambda,\lambda')$ is only of a minor importance for measurements outside of atmospheric gases absorption bands. This is not the case, of course, for absorption bands of atmospheric gases (e.g., O_2, H_2O, CO_2, N_2O, CH_4), which have an extremely complicated structure. The task of this paper is to model TOA spectra both outside and inside gaseous spectral bands. Thus, the precise shape of $f(\lambda,\lambda')$ cannot be ignored. We, therefore, develop here the approximation for the monochromatic intensity $I(\lambda,\vartheta_0,\vartheta,\varphi)$ or, more precisely, for the monochromatic reflection function $R(\lambda,\vartheta,\vartheta_0,\varphi)=I(\lambda,\vartheta,\vartheta_0,\varphi)/F\cos\vartheta_0$. This allows to use the results presented below for any types of the response functions $f(\lambda,\lambda')$.

The TOA reflectance R can be presented as a sum of two terms:

$$R=R_1+TR_2, \tag{2}$$

where R_1 describes light scattering and radiative transfer in the atmosphere above a cloud (with account for both gaseous and particle scattering and absorption). The value of R_2 is due to

cloud-underlying atmosphere and surface contribution (see Fig. 1). We omit arguments in functions in Eq. (2) for the sake of simplicity. The multiplier T accounts for the extinction of the direct solar light on the path from the sun to the cloud top and from there to a receiver.

The scattering of light above clouds is rather weak. Thus, we will calculate the value of R_1 in the single scattering approximation [1]:

$$R_1 = \frac{1}{4\xi\eta}\int_0^{h-H} \mathrm{d}z(\sigma_{\mathrm{sca}}^{\mathrm{R}}(z)p^{\mathrm{R}}(\theta) + \sigma_{\mathrm{sca}}^{\mathrm{A}}(z)p^{\mathrm{A}}(\theta))\exp[-\tau(z)(\xi^{-1}+\eta^{-1})], \tag{3}$$

where $\sigma_{\mathrm{sca}}^{\mathrm{R,A}}(z)$ are Rayleigh and aerosol scattering coefficients, respectively, $p^{\mathrm{R,A}}(\theta)$ are Rayleigh and aerosol phase functions, τ is the optical thickness of atmosphere above cloud along the vertical axis OZ (see Fig. 1), directed to the Earth surface, and h is the TOA height, assumed to be equal 60 km in this study. The value of τ includes the contribution from the molecular and aerosol scattering and absorption. Also we introduced here the values of ξ and η : $\xi = \cos\vartheta_0$, $\eta = |\cos\vartheta|$.

It should be pointed out that coupling between atmospheric layers above and below cloud-top-height is neglected in Eq. (2). To account partially for this coupling and multiple light scattering above cloud top, we assume:

$$T = \exp[-\tau'(\xi^{-1}+\eta^{-1})], \tag{4}$$

where

$$\tau' = \sum_{i=1}^{N}\int_0^{h-H} C_{\mathrm{abs},i}^{\mathrm{G}}(z)c_i(z)\,\mathrm{d}z. \tag{5}$$

Here $C_{\mathrm{abs},i}^{\mathrm{G}}(z)$ is the ith gas absorption cross section, N the total number of gases present and c_i the ith gas concentration. Only extinction due to light absorption by gases is present in τ'.

Actually, the value of τ' should include also extinction by aerosol particles (the optical thickness τ^{A}) and molecules (the optical thickness τ^{R}). We neglect them in Eq. (5). This results in increase of T and the term TR_2 in Eq. (2), which partially compensates for multiple light scattering in the layer above cloud, which otherwise is completely neglected in this study. Note, that this is a standard method for a partial account of multiple light scattering effects in the problems of the atmospheric correction. However, the definition of τ' in Eq. (4) differs, depending on the problem and spectral range studied [5–7].

Now we consider the term R_2. The general expression for this term for the cloud-underlying Lambertian surface is well-known [4]. It has the following form:

$$R_2(\vartheta,\vartheta_0,\varphi) = R_{\mathrm{c}}(\vartheta,\vartheta_0,\varphi) + \frac{At_{\mathrm{c}}(\vartheta_0)t_{\mathrm{c}}(\vartheta)}{1-Ar_{\mathrm{c}}}, \tag{6}$$

where $R_{\mathrm{c}}(\vartheta_0,\vartheta,\varphi)$ is the cloud reflection at $A=0$, $t_{\mathrm{c}}(\vartheta)$ is the diffused transmittance of a cloud layer [4] and r_{c} is the spherical albedo of a cloud. We also define the cloud total transmittance: $t_{\mathrm{c}} = 1 - r_{\mathrm{c}}$.

Convenient approximate equations for R_{c}, t_{c}, and r_{c} were obtained in many studies [1,4,8–11]. Those given in [11] and used in this study are summarized in the appendix. Eqs. (2), (3), (6) do not completely solve the problem we face. We have an aerosol–gaseous medium between underlying

surface and cloud (see Fig. 1). It will influence relationship (6), obtained for the case of a transparent layer between cloud and a ground surface.

To approximately account for this influence we substitute A in Eq. (6) by the following equation:

$$A^* = r_a + \frac{At_a^2}{1 - Ar_a}, \tag{7}$$

where r_a is the spherical albedo of aerosol layer between cloud and a underlying surface and t_a is the aerosol total transmittance ($t_a = 1 - r_a$ for non-absorbing aerosols). Eq. (7) is analogous to Eq. (6). To show this, we integrate Eq. (6) over angles ϑ_0, ϑ and φ. Then it follows [10]:

$$r_2 = r_c + \frac{At_c^2}{1 - Ar_c}, \tag{8}$$

which is similar to empirical Eq. (7). Note that $r_2 = r_c$ ($A = 0$). In essence, approximation (7) allows to substitute an aerosol-underlying surface layer by an effective Lambertian surface with albedo A^*.

Clearly, we have at $r_a = 0 : A^* \equiv A$, where it is assumed that most of atmospheric aerosols are weakly absorbing and $t_a = 1 - r_a$. Thus, for calculation of A^* we should find the value of r_a (see Eq. (7)). Accounting for the fact that aerosol optical thickness is usually small and contribution to the TOA reflectance from the cloud underneath is low, we expect that rather coarse approximations for the calculation of r_a can be used. In particular, one can obtain in the single scattering approximation [12]:

$$r_a = \omega_0 \int_0^1 \xi \, d\xi \int_0^1 \eta \, d\eta \, F(\xi, \eta) \bar{p}(\xi, \eta), \tag{9}$$

where

$$F(\xi, \eta) = \frac{1 - \exp[-\tau^A(\xi^{-1} + \eta^{-1})]}{\xi + \eta} \tag{10}$$

and

$$\bar{p}(\xi, \eta) = \frac{1}{2\pi} \int_0^{2\pi} p^A(\theta) \, d\varphi. \tag{11}$$

Here

$$\theta = \arccos(-\xi\eta + \sqrt{(1 - \xi^2)(1 - \eta^2)} \cos\varphi) \tag{12}$$

is the scattering angle and τ^A is the aerosol optical thickness beneath the cloud.

It was shown [12] that under assumption $\tau^A \to 0$ Eq. (9) is reduced to a simple function expressed via the elliptic integral

$$K(p) = \int_0^{\pi/2} \frac{d\theta}{\sqrt{1 - p \sin^2\theta}}. \tag{13}$$

Namely, it follows:

$$r_a = 2\omega_0 \bar{\beta} \tau^A, \tag{14}$$

where

$$\bar{\beta} = \frac{1-g}{2g}\left\{\frac{2K(g^2)}{\pi} - 1\right\} \tag{15}$$

is so-called backscattered fraction and g is the asymmetry parameter:

$$g = \frac{1}{2}\int_0^{\pi} p(\theta)\sin\theta\cos\theta\,\mathrm{d}\theta. \tag{16}$$

Eq. (15) is exactly applicable to the case of the Heney–Greenstein phase function:

$$p(\theta) = \frac{1-g^2}{(1+g^2-2g\cos\theta)^{3/2}} \equiv \sum_{l=1}^{\infty}(2l+1)g^l P_l(\cos\theta), \tag{17}$$

where $P_1(\cos\theta)$ is the Legendre polynomial. However, it can be used with a high accuracy for other phase functions if g is known [12].

We present integral r_a (9) in Fig. 2 as the function of τ^A for different values of g. The value of r_a ($\tau^A = 2$) approximately coincides with r_a ($\tau^A \to \infty$) for the range of g studied. So r_a ($\tau^A = 2$) gives the contribution of the single scattering to a light reflection from a semi-infinite medium. We also see that the linear approximation (14) is valid for values of $\tau^A = 0.05$–0.1, depending on g. For larger values of τ^A the dependence $r_a(\tau^A)$ becomes non-linear. In particular, we found approximating the function $r_a(\tau^A)$, given by Eq. (9), at $g = 0.77$ and $\tau^A < 0.3$ (see Fig. 3):

$$r_a(\tau) = \omega_0[0.265\tau^A - 0.865(\tau^A)^2 + 1.164(\tau^A)^3]. \tag{18}$$

To complete the model, we should account for the light absorption of diffused light fluxes by gases present in a layer between a cloud and an "effective" underlying surface (see Eq. (7)). To do

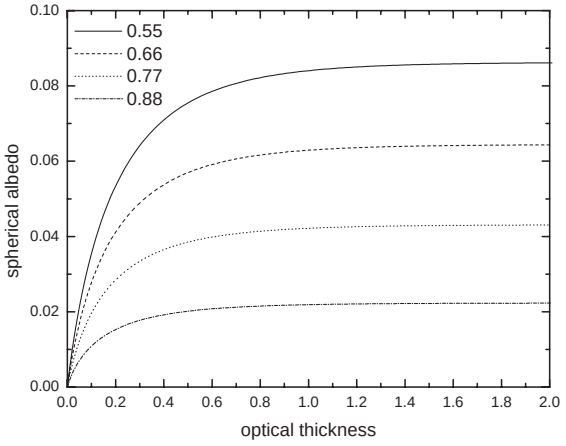

Fig. 2. The dependence $r_a(\tau^A)$, obtained with Eq. (8) at $g = 0.55,\ 0.66,\ 0.77$ and 0.88.

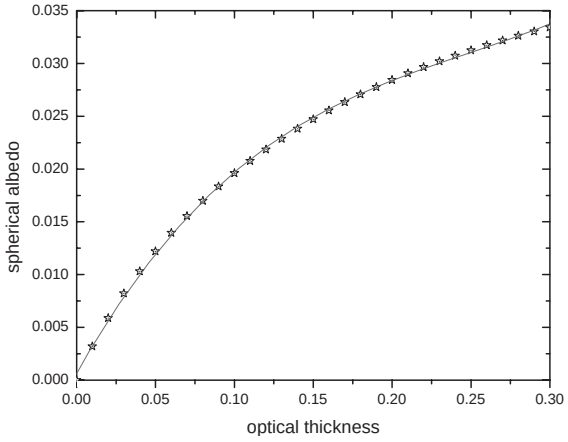

Fig. 3. The dependence $r_a(\tau^A)$, obtained with Eq. (18) (line) and Eq. (8) (starts) at $g = 0.77$.

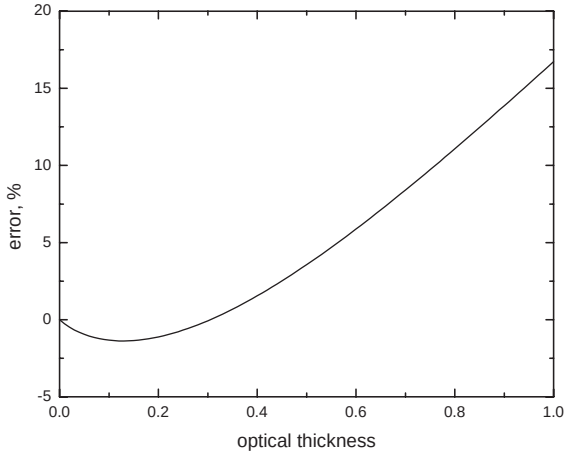

Fig. 4. The relative error of Eq. (20) as compared to Eq. (19) as function of τ^*.

so we multiply $t_c(\vartheta_0)$ and $t_c(\vartheta)$ in Eq. (6) by the flux transmittance [13,14]

$$\gamma = 2\int_0^1 d\xi\,\xi \exp\left[-\frac{\tau^*}{\xi}\right], \tag{19}$$

where τ^* is the optical thickness due to absorbing gases in a layer between a cloud bottom and a ground surface. Eq. (19) can be substituted by

$$\gamma = \exp(-\Upsilon\tau^*), \tag{20}$$

where $\Upsilon \approx 1.7$ is the so-called diffusivity factor commonly used in the transmission modeling. The accuracy of Eq. (20) is better then 2% at $\tau^* < 0.4$ (see Fig. 4). For larger values of τ^* one should perform a simple integration (19) (if the high accuracy is needed). Note that $\gamma \to 0$ as $\tau^* \to \infty$.

Summing up, we have the following final approximate relationship for the TOA reflectance:

$$R(\vartheta,\vartheta_0,\varphi)=R_1(\vartheta,\vartheta_0,\varphi)+\left[R_c(\vartheta,\vartheta_0,\varphi)+\frac{A^*\gamma^2 t_c(\vartheta_0)t_c(\vartheta)}{1-A^* r_c}\right]T, \tag{21}$$

where R_1, T, A^*, γ are given by Eqs. (3), (5), (7), (20) and approximate analytical formulae for $R_c, r_c, t_c(\vartheta_0)$ are given in the appendix.

The importance of Eq. (21) is not only in the possibility to substitute the full radiative transfer calculations in the Earth—cloudy atmosphere system by an approximate formula. Most important is that it offers a simple way for the semi-analytical solution of the inverse problem (e.g., the cloud-top-height determination). This will be a subject to our next publication, however.

3. The forward model

3.1. The radiative transfer model

Owing to the phenomenological derivation of Eq. (21), it is not possible to derive the errors introduced, using only the model presented above. Clearly, for this we need to run a full radiative transfer code for the Earth atmosphere-underlying surface system with realistic distributions of atmospheric gases and aerosols. For this study we have used the SCIATRAN radiative transfer code, developed at Bremen University [15]. The SCIATRAN code originates from the well-known and highly used in trace gas retrievals GOMETRAN model [16]. The test of SCIATRAN accuracy can be found in [17]. In particular, it was found using the DISORT model [18], that the accuracy of SCIATRAN is better than 1% for most of geometries and any cloud optical thickness. Note that calculations according to the Mie theory [10] are used as an input to SCIATRAN radiative transfer code. Those allow to find phase function, single scattering albedo and extinction coefficient as functions of particles' refractive index and particle size distributions. The cases of non-spherical particles can be also treated, but then the Mie theory should be substituted by light scattering theories valid for such scatterers [10].

We found that the standard version of SCIATRAN [16,17] has a poor accuracy (errors up to 5%) for water clouds at the rainbow and glory scattering regions. This is due to a limit number of Legendre polynomials, used in the cloud phase function representation. To overcome this problem, the following correction of SCIATRAN [16,17] was developed. First of all we have calculated the contribution of the singly scattered light I_{ss}, using the SCIATRAN model. Then we have subtracted I_{ss} from the result obtained and added the exact value of I_{ss}, which has a simple analytical form [10]. We found by comparison with published results [19] that the accuracy of this new version of SCIATRAN for cloudy atmospheres is better than 1% also for rainbow and glory geometries.

We restricted the comparison by an extremely narrow spectral range of oxygen A-absorption band (758–768 nm). It was done by purpose. This spectral range is usually applied to the cloud-top-height determination [20–23]. Thus, Eq. (21), proven to be valid, can be applied for the same purpose. Also the value of the reflection function and the atmospheric transmittance is changed practically from 0 to 1 in the band and its vicinity. This allows us to consider a very broad range of TOA reflectances, even if consider only this small spectral interval ($\Delta\lambda = 10$ nm).

The final note is related to the comparisons of exact results with approximation (21). Namely, we do not present here the comparisons for the case of monochromatic radiances. This is mainly of an

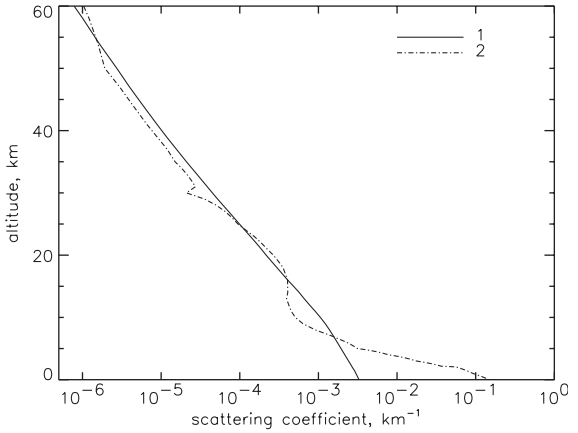

Fig. 5. The dependence $\sigma_{sca}^{A}(z)$ (broken line), $\sigma_{sca}^{R}(z)$ (solid line), used in calculations (the wavelength $\lambda = 760$ nm).

academic interest. Instead, we have used Eq. (1) to find $R_{\Delta\lambda}$ at $\Delta\lambda$=0.35 nm. This corresponds to the spectrometer GOME [26]. Note, that other spectrometers in current operation have larger values of $\Delta\lambda$. We found that the accuracy of Eq. (21) increases with $\Delta\lambda$. Thus, all estimations presented here can be considered as upper error estimations (at least as currently flying spectrometers are concerned, including most advanced SCIAMACHY spectrometer on board of ENVISAT, having $\Delta\lambda = 0.48$ nm at $\lambda = 604$–805 nm [24]). The response function has been taken in the following form:

$$f(\lambda', \lambda) = \begin{cases} 1/\Delta\lambda, & \lambda' \in [\lambda - \Delta\lambda/2, \lambda + \Delta\lambda/2], \\ 0, & \text{otherwise}, \end{cases}$$

which is a simple box function.

3.2. The model of atmosphere

The vertical distributions of aerosol and Rayleigh scattering coefficients through terrestrial atmosphere used in this study is shown in Fig. 5 at the wavelength 760 nm. The values of τ^{A} and τ^{R} were, respectively, 0.26 and 0.027 at this wavelength. Aerosol properties are taken from the LOWTRAN model [25]. The tropospheric aerosol model used corresponds to the case of maritime winter aerosol with ground visibility 23 km and boundary layer humidity 80% [25]. The stratospheric aerosol model corresponds to the so-called background aerosol [25].

We clearly see the enhanced aerosol layer around 20 km and highly pronounced boundary aerosol layer in the range 0–5 km above from the ground in Fig. 5. The vertical structure of the gas absorption coefficient is shown in Fig. 6 for wavelengths 758.025, 761.525 and 763.525 nm. The correspondent O_2 optical thicknesses are 0.0029, 43.1 and 0.26 for these wavelengths. Note a considerable change of the optical thickness over a small spectral interval (5.5 nm).

The strong absorption (see broken lines in Fig. 6) is due to oxygen. Solid line presents comparatively weak absorption by other gases (mostly ozone with the optical thickness equal to 0.004), which is identified by the peak around 20 km (see Fig. 6). The data presented in Fig. 6 and also at other wavelengths used in calculations (not shown explicitly in Fig. 6) are calculated utilizing the

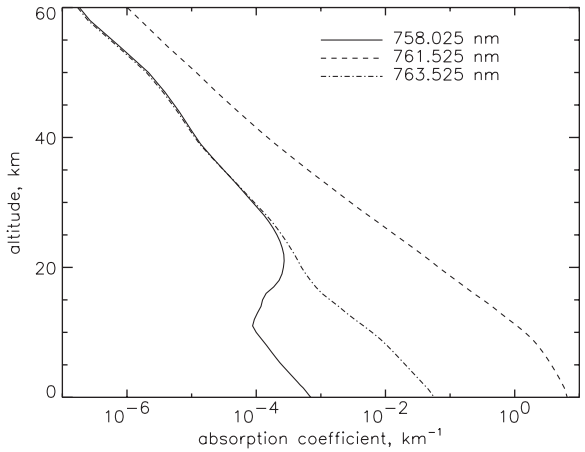

Fig. 6. The dependence of gaseous absorption coefficient on the altitude for selected values of $\lambda = 758.025,\ 761.525$ and 763.525 nm.

HITRAN 96 database of line parameters [26]. We assumed that the lines shapes are given by the Voigt function. All calculations are performed for the case of temperature and pressure profiles for the 55° latitude (January) according to the model [27].

The phase function for aerosol was taken in form (17) with values of g, depending on the height in a discrete way. In particular, we assumed that $g = 0.7731$ at $z^* < 2$ km, $g = 0.6614$ at $z^* \in [2\text{ km}, 10\text{ km}]$, $g = 0.6448$ at $z^* \in [10, 30\text{ km}]$, $g = 0.6868$ at $z^* > 30$ km. Here z^* is the attitude above the sea level.

The Rayleigh phase function was assumed to be constant with height and given by a familiar expression [28]:

$$p^{\mathrm{R}}(\theta) = \frac{3}{4 + 2\rho}[1 + \rho + (1 - \rho)\cos^2\theta], \tag{22}$$

where ρ is the depolarization factor.

The aerosol is assumed to be weakly absorbing with absorption coefficient given by the Lowtran model [25]. We do not present the correspondent dependence here due to its small influence on the TOA reflectance in the framework of the model under study.

The results presented below were obtained for the Deirmendjian's Cloud C.1 droplet distribution $f(a) = Aa^6 \mathrm{e}^{-6a/a_0}$, where $A = const$ and $a_0 = 4$ μm. We have used 50 moments of the expansion of the phase function on the Legendre polynomials. This (combined with the δ–M approach [1]) allows accurately account for the phase function angular dependence in our radiative transfer code.

The vertical distribution of the atmospheric single scattering albedo used in calculations is given in Fig. 7 for wavelengths 758.025, 761.525 and 763.525 nm. The broken line with dots near the right boundary of Fig. 7 indicates the single scattering albedo, which is due to aerosol absorption only (in the assumption that $\sigma_{\mathrm{abs}}^{\mathrm{G}} = 0$). We see that the aerosol absorption is indeed small and $\omega_0 \approx 1.0$ for the aerosol medium. The solid line presents the single scattering albedo outside the oxygen A-band. It is mostly due to ozone absorption. We see that $\omega_0 > 0.9$ at this wavelength. It is close to one in the region of heights 4–5 km, where cloud is placed. This is due to non-additivity property of

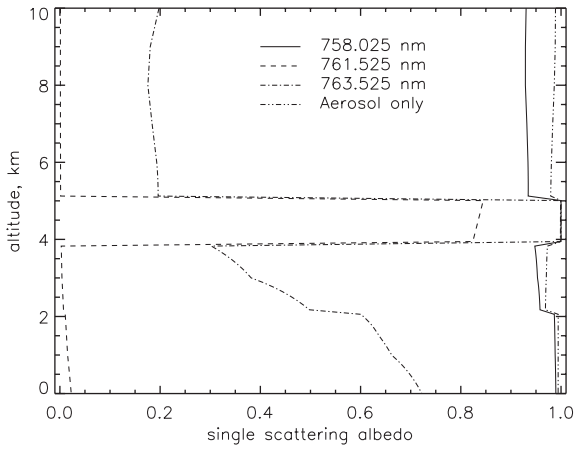

Fig. 7. The dependence $\omega_0(z)$ for three wavelengths, used in this study. The curve, with highest values of $\omega_0(z)$ corresponds to the artificial cal $\sigma_{\mathrm{abs}}^{\mathrm{G}} = 0$.

the single scattering albedo, combined with the large values of scattering coefficients of a cloudy medium.

In comparisons presented below the values of H and ΔH (see Fig. 1), however, are not fixed, but varied. It allows us to study the influence of those variations on the accuracy of main Eq. (21). Also we have varied the values of A, ϑ_0, cloud optical thickness, the aerosol type and cloud microphysical parameters. The zenith observation angle ϑ was fixed and assumed to be equal 0° (nadir observation).

Summing up, we underline that our atmospheric model is very close to a realistic scenario in the Earth atmosphere. And yet we found that the accuracy of Eq. (21) is better than 5% for most of cases studied. This is close to typical measurement errors. Some results of comparisons performed are given below.

4. The accuracy of the approximate model

4.1. The cloud optical thickness variation

First of all we study the accuracy of our approximate model in respect to the cloud optical thickness variation (see Fig. 8). The results obtained are also of a general interest.

The calculations in Fig. 8 were performed for values of cloud optical thickness 5–100, which covers the most frequent range of cloud optical thickness change [3]. We see that the TOA reflection function is extremely sensitive to the value of cloud optical thickness outside the oxygen absorption band, located at $\lambda = 758.5$ nm. It varies in the range 0.25–0.8 for the case studied. This feature is used in the cloud optical thickness determination [29,30].

The dependence of the TOA reflection function on the cloud optical thickness inside the oxygen absorption band is also of importance. In particular, for the case studied here the TOA reflection function in the center of O_2 A-band increases from 0.05 to 0.1, while cloud optical thickness changes

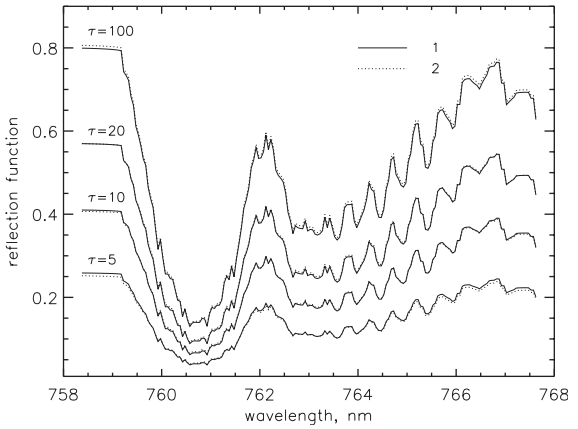

Fig. 8. The dependence of the TOA reflection function $R(0^\circ, 60^\circ)$ on the wavelength in the oxygen A-band for the atmospheric model, specified in the text at $\Delta H = 1$ km, $H = 5.5$ km, $A = 0$ and several values of cloud optical thickness $\tau_c = 5, 10, 21, 100$ (1—exact calculations for the Earth-cloudy atmosphere system, 2—calculations according to Eq. (21)).

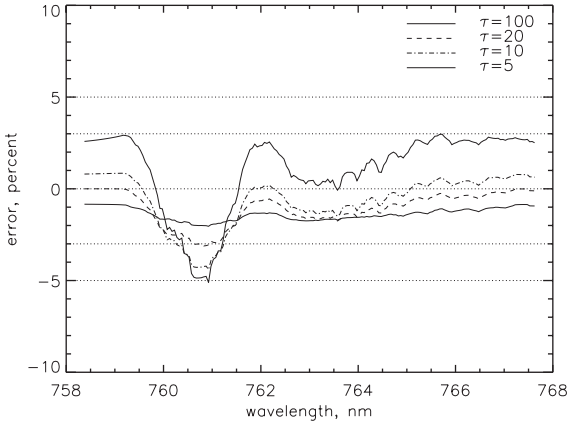

Fig. 9. The relative error of Eq. (21) $\varepsilon \equiv 100(1 - R/R^*)$, where R is obtained from Eq. (21) and R^* from exact radiative transfer calculations for the case given in Fig. 8.

from 5 to 20. Thus, to derive cloud-top-height from the depth of the absorption line around 761 nm, one should know also the value of τ_c.

We see that approximate Eq. (21) describes correctly all characteristic features of the spectral behavior of the TOA reflectance function. The error of Eq. (21) is given in Fig. 9.

It follows from Fig. 9 that the accuracy of Eq. (21) is in the range $[-5\%, 3\%]$ for the cloud layer of 1 km thickness and the top height equal to 5.5 km. Such a high accuracy is hardly expected, taking into account the phenomenological derivation given above. It, therefore, confirms our physical arguments concerning the significance of different contributions to the TOA reflectance.

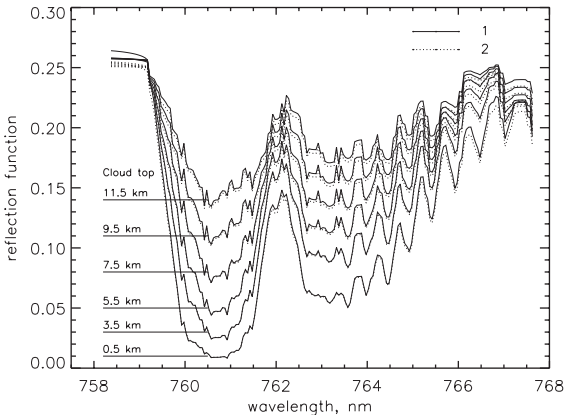

Fig. 10. The same case as in Fig. 8, but at $A=0, \Delta H=0.25$ km, $\tau_c=5$ and several values of $H=0.5, 3.5, 5.5, 7.5, 9.5, 11.5$ km.

Similar accuracy was obtained for other solar angles in the range 0–70°, other cloud droplets average radii in the range 4–16 μm and other realistic extinction coefficients of a boundary aerosol layer with the meteorological visibility range 10–50 km (not shown here).

4.2. The cloud-top-height variation

The dependence of R on the cloud-top-height is given in Fig. 10. The results were obtained at $\tau=5, \Delta H=0.25$ km, $\vartheta_0=60°$. We see that the TOA reflectance increases with cloud-top-height from $R=0.01$ (at $H=0.5$ km) till $R=0.14$ (at $H=11.5$ km) in the center of the absorption line. The increase is in more than order of magnitude. This fact is used for cloud-top-height monitoring from satellites [20–23].

The physical origin of the TOA reflectance dependence on the cloud type height around $\lambda=761$ nm is clear. It is due to high reflection of light from a cloudy medium. This does not permit photons to penetrate to deep atmospheric layers and be trapped there by oxygen molecules.

The results of comparisons of calculation of the TOA reflection function, using Eq. (21) and exact theory, is presented in Fig. 10. We see that Eq. (21) correctly describes the dependence of R on the cloud-top-height. The correspondent errors are given in Fig. 11. Note that errors are smaller than 4% even for low clouds with cloud-top-height equal to 0.5 km. The error decreases down to 2.5% for clouds with cloud-top-height 11.5 km. It suggests that the single scattering approximation is a valid approximation even if clouds are absent, $A=0$, and $\lambda=758$–768 nm. Most probably this is due to a high light absorption in oxygen A-band, which reduces multiple scattering effects in a clear atmosphere. This is confirmed by numerical experiments at $\lambda=758$–768 nm and $A=0$. Note, that the accuracy of single scattering approximation decreases with the value of A due to additional illumination of atmosphere from the ground.

In conclusion, we underline that the accuracy of Eq. (21) inside the oxygen band depends also on the cloud geometrical thickness. It follows from Fig. 11 that the accuracy of Eq. (21) is 0.5% in the center of the oxygen band at $H=5.5$ km. This is in contrast with 5% error for the same conditions (e.g., the same value of τ_c), but different cloud geometrical thickness, given in Fig. 9.

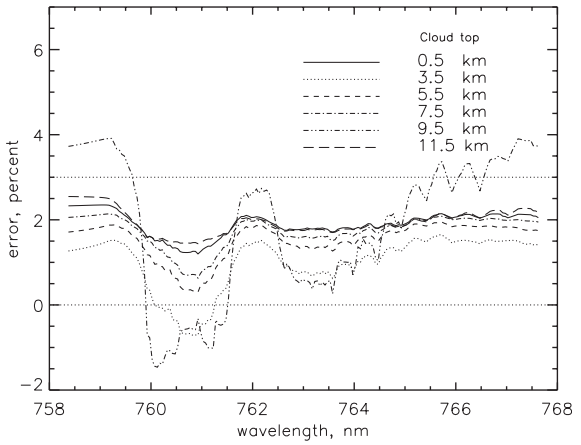

Fig. 11. The relative error ε for the case presented in Fig. 10.

Cloud geometrical thickness for data given in Fig. 9 is 1 km as compared to only 0.25 km for the case, given in Fig. 11. It means that the cloud extinction coefficient is large for the case, given in Fig. 11. Absorption coefficient is, however, the same for both cases. It means that the ratio absorption/extinction is larger for the case given in Fig. 9. This is a genuine reason for the difference in errors for both cases. Eq. (21) becomes more accurate with decrease in the level of absorption. This is mostly due to the application of formulae given in the appendix. Their accuracy decreases with $1-\omega_0$, where ω_0 is the single scattering albedo [11].

Data given in Fig. 10 can be used for the cloud-top-height estimation from measurements of the reflection function. Note that it is of advantage to use relative values in the estimation of H. In particular, we can introduce the relative band depth:

$$\Theta = \frac{R(\lambda_1) - R(\lambda_2)}{R(\lambda_1)} \tag{23}$$

or

$$\Theta = 1 - \mathbb{Q}^{-1}, \tag{24}$$

where

$$\mathbb{Q} = \frac{R(\lambda_1)}{R(\lambda_2)}. \tag{25}$$

Here λ_1 is the wavelength outside of the band and λ_2 is the wavelength inside the absorption band. Clearly, we have: $\mathbb{Q} > 1$. The dependence of $\mathbb{Q}$ on the cloud-top-height is given in Fig. 12a both using SCIATRAN radiative transfer solver and approximate equation (21). We assumed that $\lambda_1 = 758$ nm and $\lambda_2 = 763$ nm. Also we used: $\Delta H = 0.25$ km$(\tau = 5)$ and $\Delta H = 1.0$ km$(\tau = 20)$. Other input parameters coincide with those used in Fig. 8. We found that the relative error of Eq. (21) is less than 3.5% for the case given in Fig. 12a both for τ equal to 5 and 20. This is very promising result as far as cloud-top-height retrievals, using our approximation, are concerned. They

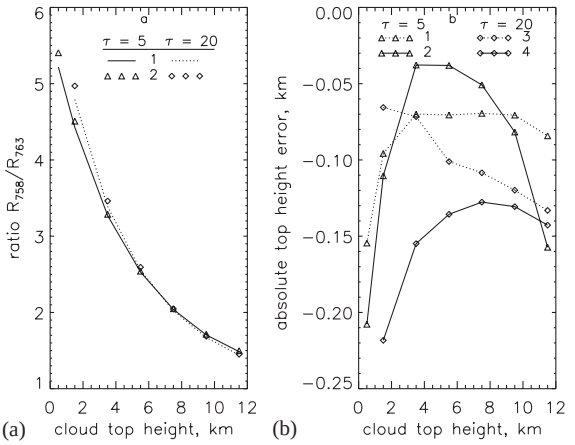

Fig. 12. (a) The dependence of the ratio $R(758\text{ nm})/R(763\text{ nm})$ on cloud-top-height H at $\tau = 5(\Delta H = 0.25\text{ km})$ and $\tau = 20(\Delta H = 1\text{ km})$. Other conditions as in Fig. 8. Lines give approximate results. Points are obtained using SCIATRAN. (b) The dependence of the absolute cloud-top-height error Ψ on the value of the cloud-top-height H obtained with Eq. (26) (lines 2,4) and Eq. (28) (lines 1,3). Other input parameters as in (a).

will be treated in a separate publication. However, for the sake of completeness, we show in Fig. 12b the absolute accuracy of the cloud-top-height determination with approximate theory developed here, using SCIATRAN data presented in Fig. 12a as measured ratios. Solid lines in Fig. 12b give absolute cloud-top-height error $\Psi = H_1 - H_2$, where H_1 is the measured (or, more exactly, obtained from the exact SCIATRAN model) cloud-top-height and H_2 is the cloud-top-height obtained from the application of our approximate theory. More precisely, in calculations of ε, we have used the following relationship:

$$\Psi = \frac{\Theta_1 - \Theta_2}{\dot{\Theta}}, \tag{26}$$

where $\dot{\Theta}$ is derivative of Θ with respect to H, Θ_1 is the value of Θ obtained from the SCIATRAN (see Fig. 12a) and Θ_2 is the same value, which follows from our approximate theory (see Fig. 12a). We see that the absolute error is negative. Therefore, our approximate theory overestimates the value of H. This overestimation is not larger than 0.25 km for cloud-top-heights in the range 0.5–11.5 km. Clearly, the correspondent relative error decreases rapidly with H.

Note that the value of Ψ can be reduced if more spectral channels (and not only λ_1, λ_2) are used. To illustrate this we introduce the logarithm

$$\Xi(\lambda) = \ln\left\{\frac{R_1(\lambda)}{R_2(\lambda)}\right\}, \tag{27}$$

where subscripts have the same meaning as in Eq. (26). Then the value of Ψ can be obtained minimizing the quadratic form

$$\left\| \Xi(\lambda) - \frac{\mathrm{d}\ln R_2(\lambda)}{\mathrm{d}H}\Psi \right\|^2 \to \min. \tag{28}$$

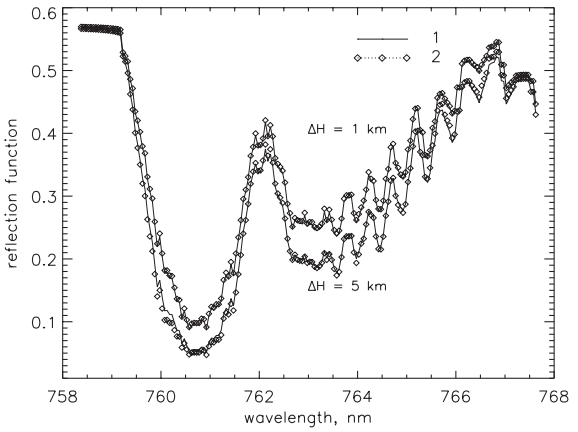

Fig. 13. The same as in Fig. 8, but at $\tau_c = 20$ and $\Delta H = 1$ and 5 km.

The results of this procedure at the wavelength range 758–768 nm (other parameters as in Fig. 12a) are given in Fig. 12b by dashed lines. We see that this approach allows to reduce the absolute error of the cloud-top-height determination to values smaller than about 150 m for values of H in the range 0.5–12 km.

4.3. The cloud geometrical thickness variation

The cloud optical thickness τ_c is defined as the product of the cloud geometrical thickness ΔH and the cloud extinction coefficient σ_{ext}. It means that clouds, having the same value of τ_c, but different values of ΔH, will have different values of the extinction coefficient, as discussed above. In particular, the extinction coefficient is larger for geometrically thinner clouds at $\tau_c = \text{const}$. As it was discussed above, it leads to smaller values of the single scattering albedo for geometrically thicker clouds. Thus, we note that the increase in cloud geometrical thickness at $\tau_c = \text{const}$ should lead to the decrease of the TOA reflection function.

These arguments are confirmed by data given in Fig. 13, obtained for various values of ΔH and $\tau = 20, \vartheta_0 = 60^\circ, A = 0$. We see, therefore, that the dependence $R(\Delta H)$ cannot be ignored. For instance, the increase of ΔH from 1 to 5 km leads to a two-fold decrease of the TOA reflection function (from 0.1 to 0.05 at $\lambda = 760.5$ nm). Large variations of R occur at the wavelength 763 nm, where they reach 30%. Thus, the cloud-top-height retrieval algorithms should incorporate also the value of ΔH estimation (e.g., from the water vapor absorption band around 938 nm [23]). On the other hand, knowing the value of H (e.g., from the Ring effect [31]), one can obtain also ΔH from measurements in the oxygen A-band. The accuracy of Eq. (21), given in Fig. 14, appears to be high as well for this case. It is in the range $[-3\%, 3\%]$ for $\Delta H = 1$ and 3 km. The error sharply increases around $\lambda = 761$ nm and $\Delta H = 5$ km. However, this case is presented for illustration purposes only. First of all clouds with $\tau = 20$ do not have the thickness around 5 km. They are much thinner.

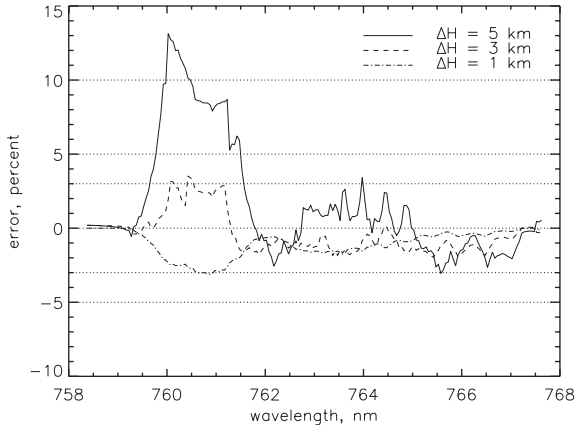

Fig. 14. The relative error ε for the case presented in Fig. 13.

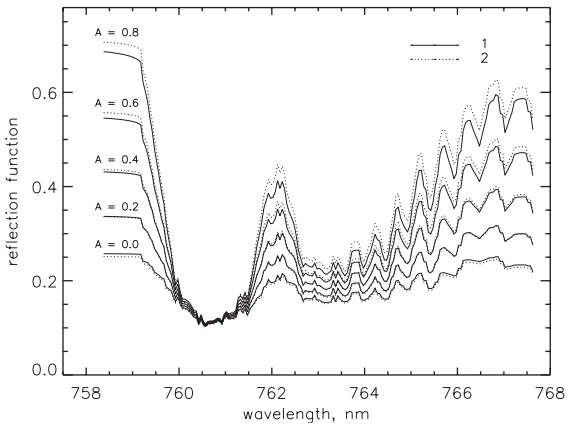

Fig. 15. The same as in Fig. 8, but at $\Delta H = 0.25$ km, $H = 9.5$ km, $\tau_c = 5$ and several values of $A = 0, 0.2, 0.4, 0.6, 0.8$.

4.4. The surface albedo variation

We present results of the calculation of the reflection function in the oxygen A-band for different Lambertian ground albedo and $\tau = 5$ in Fig. 15. We assumed that cloud geometrical thickness is equal to 0.25 km the cloud-top-height is equal to 9.5 km and $\vartheta_0 = 60°$. Note, that effects of ground albedo are of smaller importance for larger values of cloud optical thickness.

In the center of the oxygen A-band, the variation of the surface albedo almost does not influence the TOA reflectance. Outside the oxygen absorption band the influence of the surface albedo is important. We found that the variation of albedo from 0 to 0.8 leads to approximately the same variation of TOA reflectance as due to the variation of the cloud optical thickness from 5 to 100 (compare Figs. 8 and 15).

The comparison of exact and approximate calculations show that Eq. (21) grasps all important features of TOA reflectance variation inside the oxygen A-band, depending on the ground albedo (see Fig. 15).

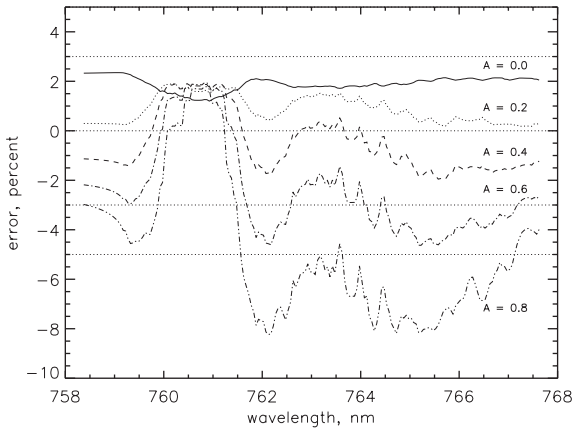

Fig. 16. The relative error ε for the case presented in Fig. 15.

The accuracy of Eq. (21) is smaller than 8% (see Fig. 16) even for very bright surfaces with $A=0.8$, which roughly corresponds to snow fields. It is in the range 2% for $A=0.4$, which is typical for deserts.

5. Conclusion

In conclusion, we present here a simple physical parametrization (21) for the TOA reflectance. This parametrization can be used to avoid calculations of the TOA reflectance over cloud scenes, using exact radiative transfer codes.

The error of Eq. (21) in most cases is smaller than 5%, which allows its use also for the solution of the inverse problem, namely for the determination of τ, H and ΔH.

Most of comparisons have been given for a practically important spectral band 758–765 nm. However, there is no reason to expect that model will fail to reproduce experimental results for other wavelengths in visible and near-infrared (at least up to $\lambda=2.4$ μm).

Both approximate solution and exact calculations were used to study the dependence of the TOA reflection function on various parameters, such as cloud-top-height, cloud geometrical and optical thickness, ground surface albedo, illumination conditions, etc. In particular, we found that cloud geometrical thickness value cannot be ignored in cloud-top-height retrievals, using the oxygen A-band.

Acknowledgements

This work has been supported in part by the University of Bremen, the European Union Research Programme, the European Space Agency, The German Ministry of Research and Education (BMBF) and the German Space Agency (DLR). The authors are grateful to J.P. Burrows for important discussions on the subject.

Appendix A. The cloud reflection function

Reflection function of a homogeneous optically thick (optical thickness $\tau_c > 5$) cloud over a black surface (e.g., ocean) is given by the following analytical solution [8]:

$$R(\vartheta,\vartheta_0,\varphi) = R^0_\infty(\vartheta,\vartheta_0,\varphi)\exp(-uy(1-0.05y)) - (t\exp(-x) - t^*)\exp(-y)K(\vartheta_0)K(\vartheta), \tag{A.1}$$

where

$$t = \frac{\sinh y}{\sinh[y(\alpha+z)]}, \quad t^* = (4.86 - 13.08\cos\vartheta_0\cos\vartheta + 12.76\cos^2\vartheta_0\cos^2\vartheta)/\tau_c^3,$$

$$K(\vartheta) = \tfrac{3}{7}(1+2\cos\vartheta),$$

$$\alpha = 1.07, \quad x = yz, \quad y = 4\sqrt{\frac{1-\omega_0}{3(1-g)}}, \quad z = \frac{3}{4}(1-g)\tau_c.$$

The value of $R^0_\infty(\xi,\eta,\varphi)$ gives us the reflection function of a semi-infinite non-absorbing cloud. It has the following simple form at nadir geometry used in this study [8]:

$$R_\infty(\vartheta_0) = \frac{0.37 + 1.94\cos\vartheta_0}{1+\cos\vartheta_0} + \frac{p(\pi-\vartheta_0)}{4(1+\cos\vartheta_0)},$$

where p is the cloud phase function. Note, that the spherical albedo r is given by $1-t$ for non-absorbing clouds and

$$r = \frac{\sinh(x+\alpha y)\exp(-y) - \sinh(y)\exp(-x-y)}{\sinh(x+\alpha y)}$$

in the presence of absorption.

The value of g is taken to be equal 0.86, which is typical for clouds. The optical thickness is varied in the range 5–100. This is in correspondence with results [3]. The single scattering albedo ω_0 is defined by the following equation:

$$\omega_0 = 1 - \frac{\sigma_{abs}}{\sigma_{ext}},$$

where

$$\sigma_{abs} = \sigma^A_{abs} + \sigma^G_{abs} + \sigma^C_{abs},$$

$$\sigma_{ext} = \sigma^A_{ext} + \sigma^G_{ext} + \sigma^C_{ext},$$

where indices A, G and C relate correspondent value to aerosol, gas and cloud extinction or absorption coefficients. Let us assume that $\sigma^A_{abs} = \sigma^C_{abs} = 0$. Then we have

$$\omega_0 = 1 - \frac{\sigma^G_{abs}}{\sigma_{ext}}.$$

Thus, the value of ω_0 depends on the height. Eq. (A.1) for the cloud reflection is obtained, however, for the case of a vertically homogeneous layer. The dependence $\omega_0(z)$ is not particularly strong in the area, where cloud is present (see, e.g., the curve $\omega_0(z)$ at the attitude range 4–5 km in Fig. 7).

Therefore, we adopt here the model of an "effective homogeneous layer". In this case one should find the height inside the cloud at which the value of ω_0 should be taken for calculations. We assume that this height coincides with the Chamberlian's absorption length [32,33]:

$$\ell = \frac{1}{k\sigma_{\text{ext}}}, \tag{A.2}$$

where the absorption length ℓ specifies the distance (along the vertical) from the cloud top to a fixed level inside the cloud and [32]

$$k = \sqrt{3(1-g)(1-\omega_0(1/k))}. \tag{A.3}$$

Solving Eq. (A.3) numerically, we find the value of k, which should be substituted in Eq. (A.2) to find the geometrical depth ℓ, where the single scattering albedo should be taken for calculations with Eq. (A.1). We use in Eq. (A.3): $g = 0.86$. The symbol $\omega_0(1/k)$ means the single scattering albedo at the optical depth $1/k$ from the cloud top.

Note that Eq. (A.3) is solved by the method of iterations, assuming that $\omega_0(1/k)$ in the first iteration is equal to ω_0 at the cloud-top-height. Then Eq. (A.3) is used to find k. This allows to find the next approximation for $\omega_0(1/k)$, which is used in Eq. (A.3) to find a new value of k. This process is repeated until the convergence is reached.

References

[1] Thomas G, Stamnes K. Radiative transfer in the atmosphere and ocean. Cambridge: Cambridge University Press, 1999.
[2] Cahalan R. The albedo of fractal stratocumulus clouds. J Atmos Sci 1994;51:2434–55.
[3] Trishchenko A, Li Z, Chang F-L. Cloud optical depth and TOA fluxes: comparison between satellite and surface retrievals from multiple platforms. Geophys Res Lett 2001;28:979–82.
[4] Liou KN. Radiation and cloud processes in the atmosphere. Oxford: Oxford University Press, 1992.
[5] Gordon H, et al. Phytoplankton pigment concentrations in the Middle Atlantic Bight: comparison of ship determination and CZCS estimates. Appl Opt 1983;22:20–36.
[6] Wrigley RC, et al. Atmospheric correction of remotely sensed image data by a simplified model. J Geophys Res 1992;97(D17):18797–814.
[7] Wang M, King MD. Correction of Rayleigh scattering effects in cloud optical thickness retrievals. J Geophys Res 1997;102(D22):25915–26.
[8] Rozenberg GV. Optical characteristics of thick weakly absorbing scattering layers. Dok Akad Nauk SSSR 1962;145:775–7.
[9] Van de Hulst HC. Multiple light scattering: tables, formulas and applications. New York: Academic Press, 1980.
[10] Kokhanovsky AA. Light scattering media optics: problems and solutions. London: Wiley, Springer, 2001.
[11] Kokhanovsky AA, Rozanov VV. The reflection function of optically thick weakly absorbing layers: a simple approximation. JQSRT 2003;(77):165–75.
[12] Wiscombe W, Grams GW. The backscattered fraction in two-stream approximations. J Atoms Sci 1976;33:2440–51.
[13] Feigelson EM, editor. Radiation processes in the earth atmosphere. Leningrad: Gidrometeoizdat, 1981.
[14] Li J. Accounting for overlap of fractional cloud in infrared radiation. QJR Meteorol Soc 2000;126:3325–42.
[15] Rozanov VV, et al. SCIATRAN—a new radiative transfer model for geophysical applications in the 240–2400 nm spectral range: the pseudo-spherical version. Adv Space Res 2002;29:1831–5.
[16] Rozanov VV, et al. GOMETRAN: a radiative transfer model for the satellite project GOME, the plane-parallel version. J Geophys Res 1997;102(D14):16683–95.
[17] Kurosu T, et al. Parameterization schemes for terrestrial water clouds in the radiative transfer model GEOMETRAN. J Geophys Res 1997;102(D18):21809–23.

[18] Stamnes K, et al. Numerically stable algorithm for discrete-ordinate method radiative transfer in multiple scattering and emitting layered media. Appl Opt 1988;27:2502–9.
[19] Lenoble J, editor. Radiative transfer in scattering and absorbing atmosphere. Hampton: A. Deepak, 1985.
[20] Yamomoto G, Wark DQ. Discussion of letter by A. Hanel: determination of cloud altitude from a satellite. J Geophys Res 1961;66:3596.
[21] Fisher J, Grassl H. Detection of cloud-top height from reflected radiances within the oxygen A band, Part 1: theoretical studies. J Appl Meteor 1991;114:1245–59.
[22] Fisher J, et al. Detection of cloud-top height from reflected radiances within the oxygen A band, Part 2: measurements. J Appl Meteor 1991;114:1261–7.
[23] Asano S, Shiobara M, Uchiyama A. Estimation of cloud physical parameters from airborne solar spectral reflectance measurements for stratocumulus clouds. J Atmos Sci 1995;52:3556–76.
[24] Bovensmann H, et al. SCIAMACHY: mission objectives and measurement modes. 1999;56:127–50.
[25] Kneizys FX, et al. In: Abreu LW, Anderson GP, editors. The MODTRAN 2/3 report on LOWTRAN-7 model. Contract F19628-91-C-0132 with Ontar Corp., Philips Lab., Geophys. Dir., Hancom AFB, Massachusetts, 1996. 261p.
[26] Rothman LS, et al. The HITRAN molecular spectroscopic database and HAWKS (HITRAN atmospheric workstation): 1996 edition. JQSRT 1998; 60:665–710.
[27] Bruhl Ch, Crutzen PJ. MPIC two-dimensional model. In: The atmospheric effects of stratospheric aircraft. NASA Ref. Publ., 1292, 1993. p. 103–4.
[28] Bates RP. Rayleigh scattering by air. Planet Space Sci 1984;32:785–90.
[29] King MD. Determination of the scaled optical thickness of clouds from reflected solar radiation measurements. J Atmos Sci 1987;44:1734–51.
[30] Nakajima T, King MD. Determination of the optical thickness and effective particle radius of clouds from reflected solar radiation measurements. Part 1. Theory. J Atmos Sci 1990;47:1878–93.
[31] de Beek R, et al. The Ring effect in the cloudy atmosphere. Geophys Res Lett 2001;28:721–4.
[32] Chamberlian J. The atmosphere of Venus near her cloud tops. Astrophys J 1965;141:1184–205.
[33] Yanovitskij EG. Light scattering in inhomogeneous atmospheres. New York: Springer, 1997.